

SCSP-3: A Spectrally Augmented Common Spatial Pattern Approach for Robust Motor Imagery-based Brain-Computer Interface

Sunreet Khanna, Anirban Chowdhury, *Member, IEEE*, Ashish Dutta, Venkatesh K. Subramanian

Abstract—Common spatial pattern (CSP) is a widely used method for feature extraction in motor imagery (MI)-based brain-computer interface (BCI) development. However, the performance of traditional CSP features often lacks robustness against inter-session and inter-subject variabilities present in MI-related electroencephalogram (EEG) signals. To address this limitation, we propose a novel approach to CSP-based feature extraction, combining spectral information obtained from Welch power-spectrum (PS) estimation with temporal variations which we named here as SCSP-3. Our SCSP-3 method employs independent learning paths for the temporal and spectral features extracted through CSP. We introduce a postprocessing step that crosses the classification probabilities from these pathways using element-wise products, deriving linearly separable features. The performance of SCSP-3 is evaluated and compared to the traditional CSP approach utilizing a support vector machine (SVM) for classification following a within-subject evaluation scheme. The results demonstrate a significant improvement in average accuracy for SCSP-3 with more generalizability, as it performs equally well with datasets from healthy subjects and stroke patients. This enhanced robustness and generalizability highlight the potential of SCSP-3 as a superior alternative to traditional CSP-based feature extraction methods for achieving consistent performance across different subject categories.

Index Terms—BCI, CSP, Classification, EEG, Feature extraction, Motor Imagery, SVM, Welch PS

I. INTRODUCTION

Motor Imagery (MI) is typically associated with the change in the sensorimotor rhythm (SMR) of the brain during covert limb movements, such as imagining a right- or left-hand movement [1]. Decoding the SMR related to MI bears enormous significance for neurorehabilitation after stroke as it can give neurofeedback to stroke survivors during physiotherapy [2]. A brain-computer interface is typically used for this purpose which uses advanced signal processing and machine learning techniques to decode the MI from EEG signals and controls a robotic hand orthosis device such as exoskeletons [3], [4]. However, the problem lies in the fact that the EEG signals are noisy, non-stationary, and suffer from volume conduction and artifacts which ultimately reduces its

detection accuracy significantly [5]. Over the years, many signal-processing techniques have been used to extract meaningful features of MI-related EEG signals, but the problem persists [6]. Often the proposed methods are tested on a single dataset and more often on only healthy individuals, while the primary users of the MI-BCI, the stroke patients, are excluded [7]. The feature extraction techniques involve the time domain and frequency domain representations of EEG signals. Among the purely time-domain features, autoregressive (AR) models are perhaps the most important [8]. Generally, the coefficients of the temporal dependencies within the signal are used as features in this case. Despite having some success, the AR models suffer from many issues, such as limited frequency information, insufficient spatial information, and sensitivity to noise and nonstationarities in EEG signals [9]. On the other hand, purely frequency-domain features such as power spectral density (PSD) are also widely used for MI detection as they can estimate the relative power distribution across frequency bands [10]. However, it is limited in identifying crucial transient temporal variations. Other limitations include a lack of specificity in distinguishing different MI tasks and high susceptibility to artifacts that distort the frequency pattern resulting in less accurate feature representation [11]. Nonetheless, both time and frequency domain features suffer from common problems, such as failing to capture spatial information and sensitivity to nonstationarities [12]. Hence, combined approaches of feature extraction where both temporal and frequency characteristics can be exploited are more commonly used, for example, event-related desynchronization/synchronization (ERD/ERS) [13], wavelet transform [14], and common spatial pattern (CSP) [15].

Notably, CSP can identify spatial patterns very efficiently, which contributes to enhanced feature separability by maximizing the variance of a specific class in a particular dimension while minimizing the other [16], [17]. Other advantages of using CSP involve dimensionality reduction of EEG data enhancing computational efficiency, robustness against the signal amplitude variation, and improvement of signal-to-noise ratio. Consequently, CSP became the benchmark for decoding MI-related EEG signals [18], [19], and several variants of this approach are proposed, such as filter-bank CSP (FBCSP) [20], regularised CSP (RCSP) [21], and multiclass CSP [22].

However, all these variants apply the standard technique of using temporally filtered EEG signals within a frequency band to generate the weight matrix of the CSP filter. This weight matrix is then multiplied with the band pass filtered signals

Manuscript received XXXX XX, 2023; revised XXXX XX, 2023.

(Corresponding author: Sunreet Khanna.)

S. Khanna and K. S. Venkatesh are with the Department of Electrical Engineering, IIT Kanpur, Kanpur, 208016, India (e-mails: sunreetk20@iitk.ac.in; venkats@iitk.ac.in). A. Chowdhury is with School of Computer Science and Electronic Engineering, University of Essex, Colchester, CO4 3SQ, UK (e-mail: a.chowdhury@essex.ac.uk). A. Dutta is with the Department of Mechanical Engineering, IIT Kanpur, Kanpur, 208016, India (e-mail: adutta@iitk.ac.in).

within a trial for feature extraction. One limitation of this approach is that the CSP filters depend only on the temporal variations, which do not capture the neurodynamics hidden in the frequency spectrum. The problem becomes worse when the used frequency bands are a bit larger such as the beta band, which can range from 15 Hz up to 30 Hz. Using a narrow band is also not always possible as EEG signals are known for their inter-subject variability where information content may vary across different frequencies for different subjects. Hence, we propose a fundamental change in this commonly used approach of using only temporally filtered signals for the CSP weight matrix with an additional CSP weight matrix based on the PS of the same band, which will be multiplied by the samples of the PS to generate different feature components. Thus we can take advantage of both the temporal and frequency-specific variation of the MI-related neurodynamics during spatial filtering on a more granular level. However, adding these new feature elements from PS-based CSP will increase the dimension of the feature vector, which may cause other problems during classification, such as overfitting. To encounter this challenge, we developed a postprocessing step to control the feature vector length. The temporal CSP and PS-based CSP features are held in separate feature vectors to train two different support vector machines (SVM), thereby generating two classifier models. The posterior probabilities of these classifier outputs are then fused using the Hadamard product to create a single feature vector which is then used to train the final SVM. The output of this two-stage classification architecture is then used as the predicted class of a given trial. The proposed novel feature extraction technique using PS-based CSP and the two-stage postprocessing approach combined is named SCSP-3 in the paper. The proposed signal processing and classification pipeline is tested on stroke patients' MI dataset recorded on a hand exoskeleton-based neurorehabilitation paradigm and compared against the healthy subjects dataset. Such validation is essential for the progress of neurorehabilitative BCIs as most of the newly proposed algorithms are tested primarily on healthy individuals, ignoring that the same algorithm may have drastic performance variation between healthy individuals and stroke patients. This phenomenon held back the progress of neurorehabilitative BCIs since its early days. For example, Prasad and colleagues worked on the gamification of BCI systems for stroke rehabilitation and tested them on five stroke patients. However, their accuracy was limited between 60-75% [23]. Later studies on BCI for hand rehabilitation showed that using a traditional CSP+SVM-based approach, the classification accuracy can only be improved after many repetitive sessions [24]. Adaptive BCIs with covariate shift detection also failed to produce comparable accuracies between healthy and stroke patients [5]. Gaur and colleagues proposed the longest consecutive repetition-based postprocessing of predicted labels from CSP features using a sliding window approach (SW-LCR) to address this problem. However, it is a slower process, requiring the entire trial to be windowed for making a prediction [1].

Therefore, the critical contributions of the paper are as follows:

- 1) A novel method of generating CSP filters using PS components combined with the CSP filters generated by the temporally filtered signals enhances the robustness of extracted features.
- 2) A novel postprocessing step with a two-stage SVM classification based on the posterior probabilities of the predicted labels to enhance the classification accuracy.
- 3) The performance of the novel feature extraction and classification approach on stroke patients is comparable to the healthy subjects and better than the traditional CSP-based approach.

II. MATERIALS AND METHODS

A. Dataset-A: Stroke Patients' Dataset

This dataset is generated from the EEG recordings of ten hemiparetic stroke patients undergoing the following experimental protocol. The experimental protocol consists of two sessions as follows:

1) *Training Session without Feedback*: The training phases consist of two blocks of 40 trials each. Each test lasts for 8s; from $t = 0$ s to 3 s of the trial, the subject is prompted to be ready with a 'get ready' message supplied visually. At $t = 2$ s, there is an auditory beep for a short duration, followed by a cue for the subject to attempt a left- or right-hand grasp. The grasp attempt lasts from $t = 3$ s to 8 s of the trial. Subsequent trials have an inter-trial interval (ITI) of 2 s - 3 s. The trials are equally distributed between the two classes to create a balanced dataset of 80 trials per subject [25].

2) *Online Session with Feedback*: The online trial follows the diagram in Fig. 1 where the first 3 s is the same as the trials in the training session. The cue period lasts from $t = 3$ s to 5s and is preceded by an auditory beep at $t = 2$ s. The feedback lasts from $t = 5$ s to 8 s and is provided in visual and exoskeleton-based finger motion. A computer screen provides visual feedback, whereas a hand exoskeleton device delivers proprioceptive feedback. The exoskeleton is capable of helping subjects in flexing and extending their fingers. Two servo motors move the coupled index-middle finger and the thumb in the natural finger trajectories [25]. The Institute Ethics Committee of the Indian Institute of Technology Kanpur approved the experimental protocol.

B. Dataset-B: Healthy Subjects' Dataset

The BCI Competition IV-2a dataset has been used to compare the classification results of healthy individuals performing MI tasks. This dataset has been referred to as Dataset-B for the rest of the paper. Nine healthy subjects performed MI tasks on four body parts: left hand, right hand, feet, and tongue. The training and test sessions were recorded for each subject on separate days. There were 72 trials for each class, i.e., 288 total trials per subject. Signals are sampled at a frequency of 250 Hz with an initial bandpass filter between 0.5 Hz and 100 Hz with a notch filter at 50 Hz. There were 22 Ag/AgCl electrodes following the 10-20 international system with a 3.5 cm inter-electrode distance. A trial lasts for 6 s, followed by a short break period. A fixation cross and an auditory warning were given during the first 2 s from the start of the trial.

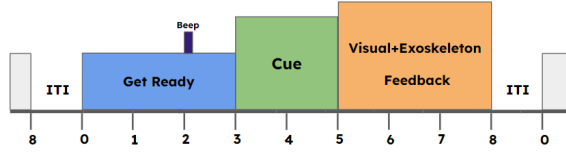


Fig. 1. The timing diagram of a trial during the online feedback phase for Dataset-A.

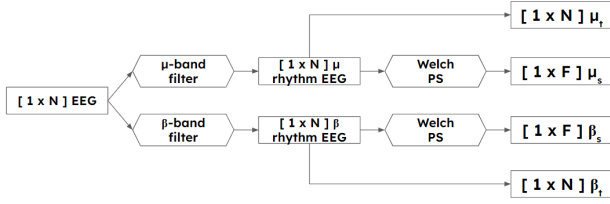


Fig. 2. Training: Block-I: The sub-pipeline above filters N sample EEG signal into its μ and β band rhythms based on the selected pass bands. Then Welch PS estimation is performed on the filtered N sample signal and produces the F length PS. Finally, four arrays are created for the next step of feature extraction, i.e., two arrays of temporally filtered EEG signal- $[1 \times N] \mu_t$ and $[1 \times N] \beta_t$; and two arrays of PS, $[1 \times F] \mu_s$ and $[1 \times F] \beta_s$

After that, a cue was presented with an arrow sign to instruct different MI tasks. Our algorithm uses the left- and right-hand MI trials as classes for our binary classification problem. This selection is made as we intend to study the performance of the classification pipeline for an upper limb motor task.

C. Signal Filtering and PS Generation

For the given experimental paradigms, T and C denote the number of trials and the number of channels, respectively. EEG signals are analyzed by investigating different frequency band components, such as the μ and β rhythms. This is based on the fact that the β rhythm has distinct topographies and responses to the limb movements compared to the μ rhythm. Thus the μ and β rhythms have been individually extracted. The μ band is defined here as 8 - 12 Hz, while two different frequency ranges were explored for the β band, namely 14 - 30 Hz and 16 - 24 Hz. The EEG signals are temporally filtered using these bandpass filters, and the PS is computed for the filtered EEG. Then we computed the CSP weight matrix from both the temporal and spectral components of the EEG signals. Finally, log-variance normalization is performed to form the feature vector. These processes are described in detail in the following sections.

A digital fourth-order Butterworth bandpass filter is used to bandpass filter the raw signals into their μ and β band rhythms. Then we apply Welch's Power Spectrum estimation method to extract spectral information for each specified frequency band, which we then processed for feature extraction [26]. Previous research has shown that during the performance of MI tasks, there is a significant change in the μ and β band power of the EEG signals, particularly a fall in the band power during the post-cue phase with recovery after approximately 2 - 3 s, which varies between subjects [27]. Therefore, for Dataset-A,

feature extraction was done over the trial duration of 0 - 8s and 3.5 - 5.5 s of the trial period. For Dataset-B, we consider the 3 - 5 s of the trial for feature extraction. After applying the Welch method to an N -sample EEG, an F -length PS is obtained, where F is given as

$$F = \lfloor N/2 \rfloor + 1 \quad (1)$$

After this process, the following data arrays are obtained:

μ_t $[1 \times N]$, μ rhythm EEG

β_t $[1 \times N]$, β rhythm EEG

μ_s $[1 \times F]$, welch PS obtained from μ_t

β_s $[1 \times F]$, welch PS obtained from β_t

The steps above are depicted as pipeline Block-I in Fig 2.

D. Spatial Filtering and Log-Variance Normalization

1) *Common Spatial Pattern*: The objective of spatial filters is to transform given data space into surrogate data space with optimized variances that enhance the differentiation between two sets of EEG signals associated with the left- and right-hand motor imagery. The approach employed to create these spatial filters relies on concurrently diagonalizing two covariance matrices.

First, we calculate the normalized spatial covariance C_{sp} for a $C \times N$ data array X , with C channels and N samples per channel as given in (2). We followed the convention of defining A' as the transpose of the matrix A .

$$C_{sp} = \frac{XX'}{\text{trace}(XX')} \quad (2)$$

For the two given groups: left-hand trials denoted by the set l and right-hand trials denoted by the set r , we have the group spatial covariance C_l and C_r respectively, calculated as the average of the group covariances. Thus the composite covariance is given by (3)

$$C_c = \overline{C}_l + \overline{C}_r \quad (3)$$

C_c can be factored using the eigenvalue decomposition into the diagonal eigenvalue matrix, λ_c , and eigenvector matrix, U_c ,

$$C_c = U_c \lambda_c U_c' \quad (4)$$

After sorting all the eigenvalues in descending order, the whitening matrix P is formed using (5), and further transformations are performed on C_l and C_r to get A_l and A_r .

$$P = \sqrt{\lambda_c^{-1}} U_c' \quad (5)$$

$$A_l = P \overline{C}_l P' \quad (6)$$

$$A_r = P \overline{C}_r P' \quad (7)$$

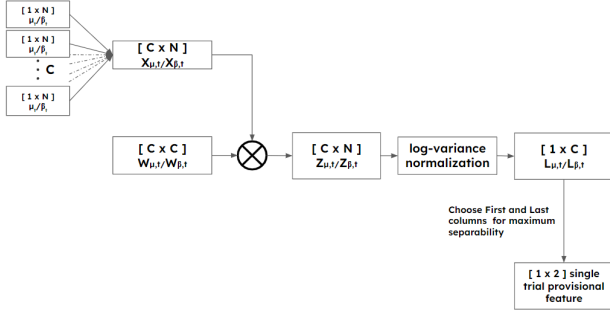


Fig. 3. Training: Block-IIa: The sub-pipeline above generates features for training the SVM classifiers. $[1 \times N]$ EEG data from C sensors are stacked to form a $[C \times N]$ data array. $[C \times C]$ CSP weight matrix transforms the sensor space into surrogate sensors space Z with dimension $[C \times N]$. Then per-channel log-variance normalization is performed, and channels with maximum separability are selected to form $[1 \times C]$ normalized features. Finally, $[1 \times 2]$ provisional feature vector is created using the first and last elements of $[1 \times C]$ for each temporal component, μ_t and β_t .

Then the eigenvalue decomposition of A_l and A_r will give us the eigenvector matrix B and eigenvalues λ_l and λ_r ,

$$A_l = B \lambda_l B' \quad (8)$$

$$A_r = B \lambda_r B' \quad (9)$$

$$\lambda_l + \lambda_r = I \quad (10)$$

where A_l and A_r have the same eigenvector matrix B and the eigenvalues of the two groups sum to 1.

The constraint in (10) implies that the largest eigenvalue for one group has the smallest eigenvalue for the other group. Thus, if we project X onto the first and the last eigenvectors of B , we will have the most optimally separable feature vectors. Thus, the decomposition of X is given as,

$$Z = (B'P)'X \quad (11)$$

$$W := (B'P) \quad (12)$$

We refer to the matrix W as the CSP weights and Z as the transformed data. Let $W_{\mu,t}$ and $W_{\beta,t}$ be the CSP weight matrices against temporal components μ_t and β_t respectively, while $W_{\mu,s}$ and $W_{\beta,s}$ be the CSP weight matrices for the spectral components μ_s and β_s respectively. Then the transformed data Z for the temporal and spectral components are obtained as follows:

$$Z_{\mu,t} = W_{\mu,t} \mu_t \quad (13)$$

$$Z_{\beta,t} = W_{\beta,t} \beta_t \quad (14)$$

$$Z_{\mu,s} = W_{\mu,s} \mu_s \quad (15)$$

$$Z_{\beta,s} = W_{\beta,s} \beta_s \quad (16)$$

2) *Log-Variance Normalization*: Given a matrix X having R rows and C columns, i.e.,

$$X \in \mathbb{R}^{R \times C} \quad (17)$$

We performed the log-variance normalization step to understand the spread of the data per row on the logarithmic scale. To do so, we perform a matrix transpose, then calculate

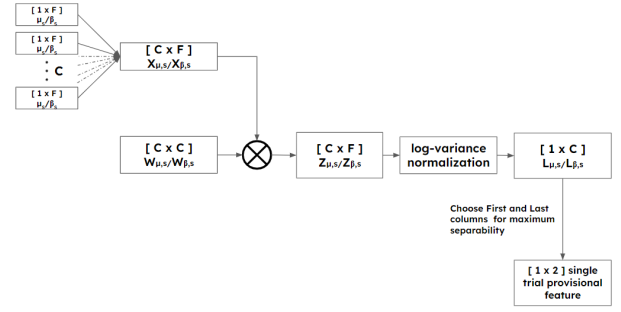


Fig. 4. Training: Block-IIb: The sub-pipeline above generates features for SVM classifiers. $[1 \times N]$ EEG data from C sensors are stacked to form a $[C \times N]$ data array. $[C \times C]$ CSP weight matrix transforms the sensor space into surrogate sensors space Z with dimension $[C \times N]$. Then per-channel log-variance normalization is performed, and channels with maximum separability are selected to form $[1 \times C]$ normalized features. Finally, the $[1 \times 2]$ provisional feature vector is created using the first and last elements of $[1 \times C]$ for each temporal component, μ_s and β_s .

variances of R different $[1 \times C]$ vectors. Then we obtained base ten logarithms on each R variance value and rescaled each log variance by the sum of all the log variances. The function $var(X)$ describes calculating the variance per column of a matrix X , and the log operation describes the real-valued base 10 logarithms as follows:

$$Y = X', Y \in \mathbb{R}^{C \times R} \quad (18)$$

$$V = var(Y), V \in \mathbb{R}^{1 \times R} \quad (19)$$

$$L[i] = \frac{\log V[i]}{\sum_{i=1}^R \log V[i]} \quad (20)$$

The CSP filtering and log variance normalization process for the temporal components μ_t and β_t is shown in Fig. 3 while the same process for the spectral components μ_s and β_s is demonstrated in Fig. 4. Thus we obtain $[1 \times C]$ normalized features from each of the four data arrays: μ_t and β_t temporal; and, μ_s and β_s spectral. Next, we select the first and the last column elements from each of the four $[1 \times C]$ normalized feature vectors based on the eigenvalue ordering described in section II-D1 to form the provisional feature vectors so that they have the maximum variance difference and hence the maximum separability between the two classes.

E. Feature Compilation and Classification

As per the scheme in Fig 5, there are four temporal and four spectral features per trial as we concatenated the $[1 \times 2]$ feature vector from the μ band with $[1 \times 2]$ feature vector from the β band for each other over T trials. Finally, we obtain a temporal feature space F_t and a spectral feature space F_s as follows:

$$F_t \in \mathbb{R}^{T \times 4} \quad (21)$$

$$F_s \in \mathbb{R}^{T \times 4} \quad (22)$$

Next, we will explain a two-step classification approach based on these two feature spaces as defined in (21) and (22). These classification steps form Block-III and Block-IV of the

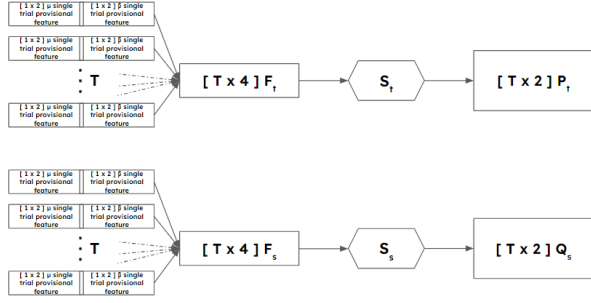


Fig. 5. Training: Block-III: The temporal CSP features from the μ and the β bands are concatenated to train the SVM model S_t while the spectral CSP features from the μ and the β bands are concatenated to train the SVM model S_s . These two different SVMs are used to generate the classification probabilities for each trial in a $(p, 1 - p)$ pair for the temporal pathway and $(q, 1 - q)$ pair for the spectral path. P_t and Q_s denote the space of p and q respectively.

pipeline, as shown in Fig. 5 and Fig. 6. As linear classifiers perform well in EEG-based MI-BCIs, we used SVM with a linear kernel to classify the features. For the sake of parity, we have chosen left- and right-hand MI classes from Dataset-B so that it matches with the classes in Dataset-A, where similar motor tasks are performed.

1) *Stage I*: We instantiate two SVM binary classifiers S_t and S_s to be independently trained on the temporal feature space F_t and spectral feature space F_s , respectively. The training paradigm performs iterative training of each SVMs with a linear kernel and uses squared L2 regularization. Let the ground truth labels be denoted by y , and the classifier function as $pclf$, which accepts two arguments: the feature space (F_t/F_s) and the SVM training model (S_t/S_s); and returns the binary label prediction probabilities. Here we use the symbols p and q to represent the predicted probability of an observation being in class 1 for the SVM training models S_t and S_s , respectively. Then we have the following training and probability prediction paradigm given in (23)-(26) for an untrained SVM object S where P_t and Q_s denote the entire space of p and q respectively.

$$(F_t, y, S) \xrightarrow{\text{train}} S_t \quad (23)$$

$$(F_s, y, S) \xrightarrow{\text{train}} S_s \quad (24)$$

$$P_t = pclf(F_t, S_t), P_t \in \mathbb{R}^{T \times 2} \quad (25)$$

$$Q_s = pclf(F_s, S_s), Q_s \in \mathbb{R}^{T \times 2} \quad (26)$$

2) *Stage II*: We further process each column of P_t and Q_s as depicted in Fig. 6 using the Hadamard product. This product performs an element-wise product of two 1-D arrays of the same length to produce another 1-D array.

Let F_p denote the newly created feature space and $F_{p,i}$ indicate the i -th column and $1_n = (1, 1, \dots, 1) \in \mathbb{R}^n$ then, as depicted in Fig. 6, we compute four new features with the

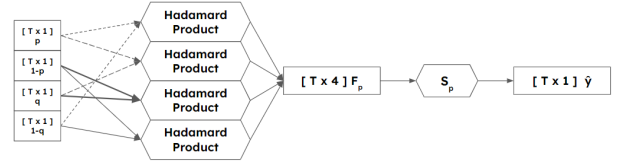


Fig. 6. Training: Block-IV: The last sub-pipeline computes features from the predicted probabilities and uses them to train the final SVM (S_p) of the pipeline. The probability arrays from Block-III are used to compute cross-classification probabilities using the element-wise product (Hadamard) per trial. The final SVM, S_p , uses these cross-products and predicts the final class labels for each trial.

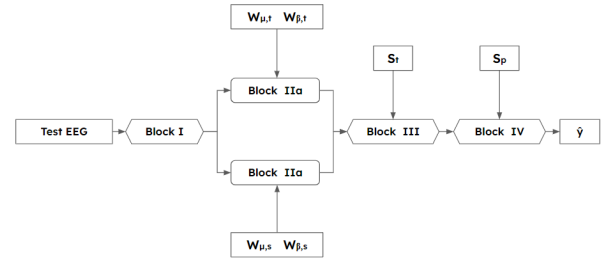


Fig. 7. Evaluation: The evaluation flow is described to the unseen assessment EEG. The blocks (as hexagons) represent the process flows during the training phase. Calculated matrices and trained objects (as rectangles) are also shown with the respective block to indicate their pre-existence (from the training phase) and not a new computation.

following heuristics

$$P_t = [P \ (1'_T - P)] \quad (27)$$

$$Q_s = [Q \ (1'_T - Q)] \quad (28)$$

$$F_{p,1} = P \odot Q \quad (29)$$

$$F_{p,2} = P \odot (1'_T - Q) \quad (30)$$

$$F_{p,3} = (1'_T - P) \odot Q \quad (31)$$

$$F_{p,4} = (1'_T - P) \odot (1'_T - Q) \quad (32)$$

In Fig. 6, p and q are single row entries for $P_{t,1}$ and $Q_{s,1}$ respectively.

The classifier learns the same task of assigning a class to each example from two versions of the data expressed in the temporal and spectral domains. The classifiers *agree* with a product of probabilities given by (29) and (32) and *disagree* on the assigned label with a product of probabilities given by (30) and (31). Using this new feature space F_p , we train a new SVM classifier object denoted by S_p from an untrained SVM binary classifier object S .

$$(F_p, y, S) \xrightarrow{\text{train}} S_p \quad (33)$$

Finally, we use the *predict* function to compute the predicted labels for each trial denoted by \hat{y}

$$\hat{y} = \text{predict}(F_p, S_p) \quad (34)$$

III. RESULTS

The performance of the proposed feature extraction and classification scheme was evaluated following the within-subject evaluation approach, as shown in Fig. 7, for both Dataset-A and Dataset-B. After completing the training pipeline, we used the subject-specific training data, such as CSP projection weights $W_{\mu,t}$, $W_{\beta,t}$, $W_{\mu,s}$, and $W_{\beta,s}$, along with the trained SVM objects S_t , S_s , and S_p to predict the outcome labels \hat{y}_e for each trial in the test data of the same subject. We calculated the classification accuracy based on the percentage agreement between each subject's predicted and ground truth labels and Cohen's Kappa (κ) values. These values were then averaged across all the subjects for comparison against the baseline method. The baseline method is defined as the method which uses traditional CSP features based on temporally filtered EEG data only and uses SVM without further postprocessing. The CSP+SVM method described in [5] without adaptation can be considered the baseline method when subject-specific selection of frequency bands and time points is not made.

A. Performance on Dataset-A

We have seen improved performance using the SCSP-3 method on Dataset-A compared to the baseline method, which uses only temporally filtered variations in EEG for CSP-based feature extraction followed by a linear SVM for classification without postprocessing. Table I showed the comparison between SCSP-3 and baseline when we took the entire trial, i.e., from 0 s to 8 s for feature extraction, while the frequency bands were chosen as 8-12 Hz for the alpha band and 16-24 Hz for the beta band. For more clarity, the comparison between the two methods for this setting is also depicted in Fig. 8. An average test accuracy of $79.25 \pm 7.73\%$ was obtained for SCSP-3, while the baseline performance was only $71.12 \pm 11.26\%$. Interestingly, the subject who scored the maximum/minimum in SCSP-3 did not score maximum/minimum for the baseline. For example, P01 got the highest accuracy in SCSP-3 with 92.5%, while P07 got the highest in the baseline with the same number. Although it failed to achieve the highest accuracy, the performance of P01 in the baseline (85%) and P07 (87.5%) in SCSP-3 were comparable and above the average. The lowest performance in SCSP-3 occurred for P06 with 65%, while the lowest for the baseline was for P05 with 55%. However, in this case, we observed that the performance for P05 in SCSP-3 was above the average at 80% while P06 got below average performance for the baseline with 67.5%. This shows the potential of SCSP-3 in improving the performance of low-scoring subjects in the baseline. A high average Kappa of 0.585 ± 0.155 ensured that the classification accuracies obtained for SCSP-3 were not biased.

Table II shows the classification accuracies for Dataset-A calculated for the trial period of 3.5-5.5s, using 8 - 12 Hz for the μ band and 14-30 Hz for the β band. For a more precise comparison between the two methods for this setting, the results are also depicted in Fig. 9. The SCSP-3 method achieved much higher classification accuracy ($76.25 \pm 10.09\%$) than the baseline ($67.50 \pm 11.96\%$) in this case. The average Kappa

value for SCSP-3 was also much greater than the baseline as the average Kappa obtained for SCSP-3 was 0.525 ± 0.202 , while for the baseline method, it was only 0.350 ± 0.239 . The capability of SCSP-3 in uplifting the performance of low-scoring subjects is again evident from the fact that P06 (lowest performer for the baseline method), who achieved only chance level accuracy of 50% for the baseline method, reached a much higher accuracy of 67.5% for SCSP-3. But the reverse is invalid, i.e., the lowest performer (P08) in SCSP-3, with an accuracy of 62.5%, scored the same for the baseline method. On the other hand, the highest performers (P01 for SCSP-3 and P10 for the baseline) got comparable performance. For example, P10 achieved the same accuracy of 87.5% for both ways, while P01 achieved a bit higher performance in SCSP-3 (90%) than in the baseline (80%).

B. Performance on Dataset-B

The superiority of SCSP-3 over the baseline method is also evident in the case of healthy subjects from Dataset-B, shown in Table III. Here, the average test classification accuracy for SCSP-3 was $76.34 \pm 8.5\%$ with a kappa of 0.527 ± 0.316 , while the baseline method performed lesser than SCSP-3 with an average classification accuracy of $73.82 \pm 18.71\%$ and a kappa of 0.477 ± 0.374 . Subject P08 achieved the highest classification accuracy (94.03% for SCSP-3 and 95.22% for the baseline), while subject P05 got the lowest accuracy (52.6% for SCSP-3 and 44.44% for baseline). It is to be noted that one-third (3 out of 9 subjects) of the subjects scored very low (accuracy $< 60\%$) in the case of the baseline method, while for SCSP-3, this number is only at 11.11% (1 out of 9 subjects). For more clarity, Fig. 10 gives a comparative bar graph for the test accuracies for SCSP3 versus the baseline for Dataset-B.

IV. DISCUSSION

The current study introduces a novel approach to extracting CSP features using P components and the traditional bandpass-filtered time series. It combines them using a novel post-processing technique of fusing classifier outputs to enhance the decoding accuracy of MI-related EEG signals for BCI applications. The strength of the proposed approach lies in using the μ and β band Ps to generate CSP filters. This is a frequency domain approach, whereas traditionally, band pass filtered signals for μ and β bands in the time domain were used to generate the CSP filters. The novelty has also been introduced in the classification approach, where we considered the posterior probabilities of the predictions made by the SVM classifiers for both temporal and spectral CSP feature spaces. These probabilities are then combined using the feature product technique to obtain the final predicted labels.

Another important aspect of our work is that we have tested this new algorithm for stroke patients and healthy individuals as subjects, which is rarely found in the literature [4]. Generally, stroke patients have altered neurodynamics which can generate a different activation pattern than healthy individuals, and often a higher non-stationarity is also found in such datasets [28]. The fact that the proposed method works equally well for healthy subjects and stroke patients

TABLE I

CLASSIFICATION ACCURACY (ACC) AND KAPPA VALUE (κ) COMPARISON BETWEEN SCSP-3 AND THE BASELINE (CSP+SVM) FOR THE ENTIRE TRIAL DURATION: 0 S TO 8 S WITH FREQUENCY BANDS μ =[8-12 Hz] AND β =[16-24 Hz] FOR DATASET-A.

Algorithm →	SCSP-3			Baseline Method		
Subject-ID	10CV Acc	Test Acc	κ	10CV Acc	Test Acc	κ
P01	77.5	92.5	0.85	66.25	85	0.7
P02	88.75	80	0.6	87.5	62.5	0.25
P03	82.5	85	0.7	80	62.5	0.25
P04	87.5	75	0.5	86.25	75	0.5
P05	91.25	80	0.6	88.75	55	0.1
P06	90	65	0.3	90	67.5	0.35
P07	78.75	87.5	0.75	70	92.5	0.85
P08	85	75	0.5	73.75	72.5	0.45
P09	81.25	75	0.5	80	65	0.3
P10	88.75	77.5	0.55	83.75	75	0.5
Avg	85.125	79.25	0.58	80.62	71.25	0.43
Std	4.88	7.73	0.15	8.23	11.26	0.22

TABLE II

CLASSIFICATION ACCURACY (ACC) AND KAPPA VALUE (κ) COMPARISON BETWEEN SCSP-3 AND THE BASELINE (CSP+SVM) FOR TRIAL DURATION: 3.5 S TO 5.5 S WITH FREQUENCY BANDS μ =[8-12 Hz] AND β =[14-30 Hz] FOR DATASET-A.

Algorithm →	SCSP-3			Baseline Method		
Subject-ID	10CV Acc	Test Acc	κ	10CV Acc	Test Acc	κ
P01	82.5	90	0.8	78.75	80	0.6
P02	91.25	65	0.3	86.25	52.5	0.05
P03	73.75	72.5	0.449	72.5	67.5	0.35
P04	87.5	80	0.6	83.75	65	0.3
P05	87.5	70	0.4	77.5	65	0.3
P06	90	67.5	0.35	75	50	0
P07	77.5	87.5	0.75	66.25	80	0.6
P08	78.75	62.5	0.25	66.25	62.5	0.25
P09	82.5	80	0.6	78.75	65	0.3
P10	88.75	87.5	0.75	78.75	87.5	0.75
Avg	84	76.25	0.5249	76.375	67.5	0.35
Std	5.92	10.08	0.20	6.60	11.96	0.24

TABLE III

CLASSIFICATION ACCURACY (ACC) AND KAPPA VALUE (κ) COMPARISON BETWEEN SCSP-3 AND THE BASELINE (CSP+SVM) FOR TRIAL DURATION: 3 S TO 5 S WITH FREQUENCY BANDS μ =[8-12 Hz] AND β =[16-24 Hz] FOR DATASET-B.

Algorithm →	SCSP-3			Baseline Method		
Subject ID	10CV Acc	Test Acc	κ	10CV Acc	Test Acc	κ
P01	85.55	85.82	0.716	86.26	85.11	0.702
P02	86.1	61.27	0.225	78.9	52.11	0.042
P03	96.43	93.43	0.868	95.66	91.24	0.825
P04	87.5	65.52	0.311	82.11	67.24	0.345
P05	86.1	52.6	0.055	75.26	44.44	-0.108
P06	81.44	62.96	0.26	76.14	58.33	0.166
P07	87.77	80.71	0.614	85	81.43	0.628
P08	95.38	94.03	0.88	94.62	95.22	0.91
P09	91.51	90.77	0.815	88.71	89.23	0.785
Avg	88.64	76.34	0.53	84.74	73.82	0.48
Std	4.88	15.85	0.31	7.41	18.71	0.37

indicates its robustness in extracting discriminative features against such conditions. For example, using the proposed method, we got 76.25% accuracy (Table II) for stroke patients (Dataset-A), while for healthy subjects (Dataset-B), we got 76.34% (Table III) accuracy. These performances have no statistically significant (p -value >0.05) difference, making them comparable. It can be further argued that the performance of stroke patients can be considered a bit better than that of healthy subjects as 70% of the subjects (7 out of 10 in Table II) in Dataset-A achieved an accuracy of more than 70% while in Dataset-B this figure is 55.55% (5 out of 9 in Table III). The distribution of performance across various subjects between

the patient and healthy datasets (Dataset-A and Dataset-B) is given in the box plot in Fig. 11 for better clarity. Moreover, in almost all the results, there is a reduced standard deviation in favor of the proposed method, indicating that it can handle inter-subject variabilities better. An interesting observation in Table I for stroke patients' results is that the drop in accuracy from training to testing is 5.87% for the proposed SCSP-3 method, which is much less than the baseline method where the fall is 9.37%. Such a drop in accuracy from one session to another is due to the change in the data distribution related to nonstationarity [29], which is quite common in MI-related EEG data. Therefore, a lesser drop in inter-session accuracy

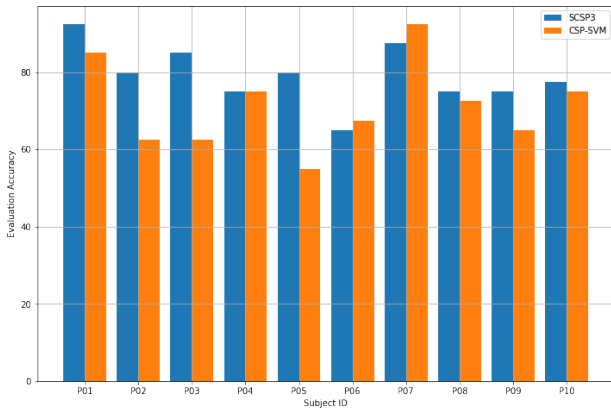


Fig. 8. Accuracy comparison between SCSP-3 and baseline (CSP+SVM) across all the subjects from Dataset-A when the entire trial period is chosen.

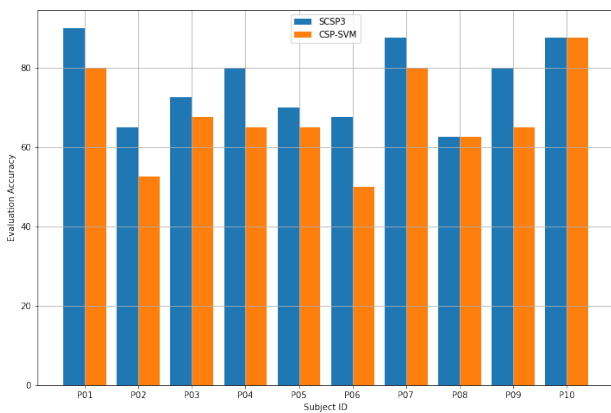


Fig. 9. Accuracy comparison between SCSP-3 and baseline (CSP+SVM) across all the subjects from Dataset-A when a particular trial segment (3.5 - 5.5 s) is chosen.

can be attributed to the greater generalizability of the extracted features by the SCSP-3 algorithm. Previous studies have used special techniques such as covariate shift adaptation to deal with the inter-session variability in accuracy, contributing to a drop of 3.88% ([5]). Thus although the proposed method has around 2% more reduction in inter-session transfer, the advantage is that, unlike covariate shift adaptation, we do not require additional computation to calculate the shift and repeated retraining of the classifier at the testing stage.

We have also compared our methods to several algorithms applied to the same dataset in the past, shown in Fig 12. The baseline method for comparison was chosen as μ and β band CSP features with SVM classifier (CSP+SVM) [30], [31], which yielded an average classification accuracy of 71.25% for the stroke patients' dataset (Dataset-A). Thus the proposed method (SCSP-3) has performed significantly (p -value <0.05) better than the baseline approach of CSP+SVM. The accuracy achieved for SCSP-3 is also significantly (p -value <0.05) more than the accuracy achieved by CSP+SVM non-adaptive classifier (NAC) [5] on the same dataset, which was an average 70.25% where the time windows and frequency bands were explicitly selected to each subject while using the baseline method. Even comparing with an adaptive version

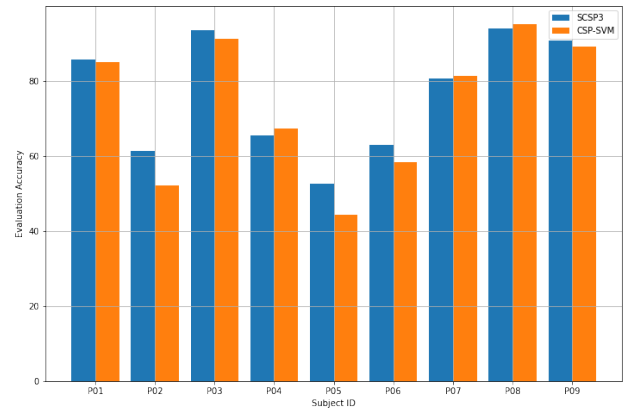


Fig. 10. Accuracy comparison between SCSP-3 and baseline (CSP+SVM) across all the subjects from Dataset-B.

(covariate shift-based adaptive classifier or CSAC) of the baseline method (average accuracy of 75.75%), reported in [5] SCSP-3 performed better (average accuracy of 79.25% in Table I). Moreover, the proposed method has also outperformed the deep learning-based (EEGNet) classification approach [7] (average accuracy of 70.25%) with a medium effect size (Cohen's $d=0.69$). The performance of SCSP-3 is also found to be superior (medium effect size, Cohen's $d=0.58$) to the recently proposed sliding-window-based CSP with longest-consecutive-repetition (SW-CSP-LCR) [1] method which reported an average accuracy of 73.5% on the same dataset. Further comparisons can be made with a recently conducted international BCI competition [2] on Dataset-A. Although the performance of SCSP-3 is only comparatively better (+0.81%) than the winner of the competition (average accuracy of 78.44%), it is much higher as compared to the second- (average accuracy of 74.69%) and third-rank (average accuracy of 73.75%) holders of the competition achieving an increase of 4.56% and 5.5% accordingly.

To show that the SCSP-3 is also compatible with a more traditional selection of time-frequency windows, for example, between 0.5s and 2.5s after the cue (here, 3.5s to 5.5s within the trial) and a wider β band of 14-30 Hz we have given the results in Table-II. This shows that the proposed method can significantly (p -value <0.05) outperform the baseline method for the same time-frequency window selection with +8.75% higher accuracy. SCSP-3 has also achieved a much higher kappa value of 0.52 compared to the baseline kappa of 0.35, which indicates a balanced prediction accuracy across the two classes in favor of the proposed method. The results on the healthy subjects' dataset (Dataset-B) are also consistent with the patients' dataset (Dataset-A) as the average accuracy across the nine subjects (in Table III) is significantly (p -value <0.05) better than the baseline method. Notably, the achieved kappa value (0.53) in this case is similar to Dataset-A.

V. CONCLUSION

The paper introduces a novel technique (SCSP-3) for extracting CSP features using P, combined with a postprocessing technique of fusing classifier outputs to enhance the decoding

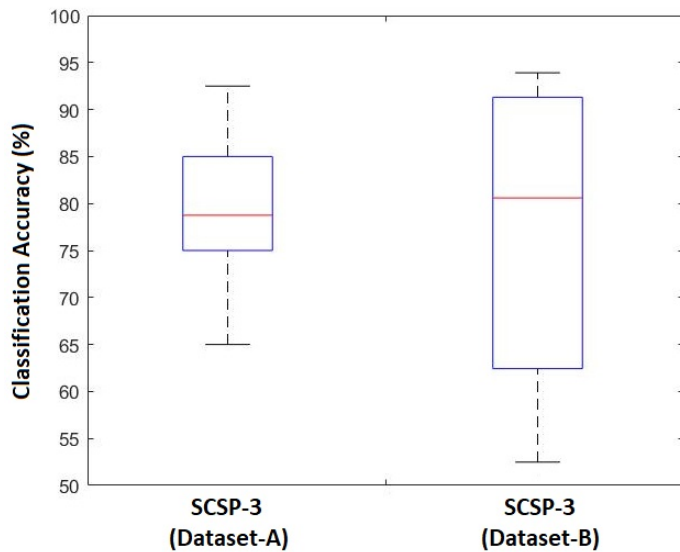


Fig. 11. Boxplot comparing the distribution of test accuracies between the Stroke patients (Dataset-A) and the healthy subjects' (Dataset-B).

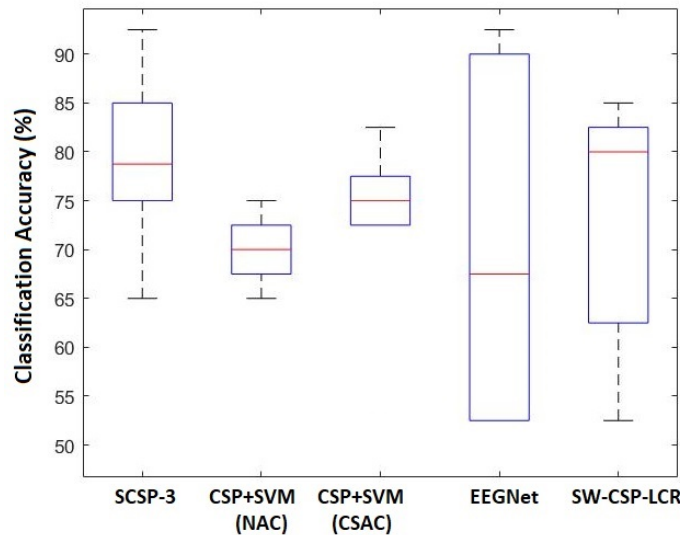


Fig. 12. Boxplot compares the distribution of test accuracies between SCSP-3 and other methods applied on Dataset-A in the past.

accuracy of MI-related EEG signals. The results have shown that SCSP-3 has performed better than the traditional approach of CSP+SVM and other comparable methods, not only in the case of healthy subjects but also for stroke patients, which is rarely found in the literature. Hence, the proposed methodology can be a significant step toward realizing robust BCI systems for stroke rehabilitation with improved accuracy. Also, the fact that it performed similarly in both datasets shows its potential for being a generalized approach to decoding MI signals across various categories of BCI users.

REFERENCES

- [1] P. Gaur, H. Gupta, A. Chowdhury, K. McCreddie, R. B. Pachori, and H. Wang, "A sliding window common spatial pattern for enhancing motor imagery classification in eeg-bci," *IEEE Transactions on Instrumentation and Measurement*, vol. 70, pp. 1–9, 2021.
- [2] A. Chowdhury and J. Andreu-Perez, "Clinical brain–computer interface challenge 2020 (cbci2020): Overview, methods and results," *IEEE Transactions on Medical Robotics and Bionics*, vol. 3, no. 3, pp. 661–670, 2021.
- [3] P. Saideepthi, A. Chowdhury, P. Gaur, and R. B. Pachori, "Sliding window along with eegnet based prediction of eeg motor imagery," *IEEE Sensors Journal*, pp. 1–1, 2023.
- [4] P. Gaur, A. Chowdhury, K. McCreddie, R. B. Pachori, and H. Wang, "Logistic regression with tangent space-based cross-subject learning for enhancing motor imagery classification," *IEEE Transactions on Cognitive and Developmental Systems*, vol. 14, no. 3, pp. 1188–1197, 2022.
- [5] A. Chowdhury, H. Raza, Y. K. Meena, A. Dutta, and G. Prasad, "On-line covariate shift detection-based adaptive brain–computer interface to trigger hand exoskeleton feedback for neuro-rehabilitation," *IEEE Transactions on Cognitive and Developmental Systems*, vol. 10, no. 4, pp. 1070–1080, 2018.
- [6] V. P. Oikonomou, K. Georgiadis, G. Liaros, S. Nikolopoulos, and I. Kompatsiaris, "A comparison study on eeg signal processing techniques using motor imagery eeg data," in *2017 IEEE 30th International Symposium on Computer-Based Medical Systems (CBMS)*, 2017, pp. 781–786.
- [7] H. Raza, A. Chowdhury, and S. Bhattacharyya, "Deep learning based prediction of eeg motor imagery of stroke patients' for neuro-rehabilitation application," in *2020 International Joint Conference on Neural Networks (IJCNN)*, 2020, pp. 1–8.
- [8] Z. Liu, L. Wang, S. Xu, and K. Lu, "A multiwavelet-based sparse time-varying autoregressive modeling for motor imagery eeg classification," *Computers in Biology and Medicine*, vol. 155, p. 106196, 2023.
- [9] S. Dutta, M. Singh, and A. Kumar, "Automated classification of non-motor mental task in electroencephalogram based brain-computer interface using multivariate autoregressive model in the intrinsic mode function domain," *Biomedical Signal Processing and Control*, vol. 43, pp. 174–182, 2018.
- [10] C. Kim, J. Sun, D. Liu, Q. Wang, and S. Paek, "An effective feature extraction method by power spectral density of eeg signal for 2-class motor imagery-based BCI," *Medical & Biological Engineering & Computing*, vol. 56, no. 9, pp. 1645–1658, 2018.
- [11] P. Herman, G. Prasad, T. M. McGinnity, and D. Coyle, "Comparative analysis of spectral approaches to feature extraction for eeg-based motor imagery classification," *IEEE Transactions on Neural Systems and Rehabilitation Engineering*, vol. 16, no. 4, pp. 317–326, 2008.
- [12] L. Zheng, Y. Ma, P. Lian, Y. Xiao, Z. Yi, Q. Song, W. Feng, and X. Wu, "A power spectrum pattern difference-based time-frequency sub-band selection method for mi-eeg classification," *IEEE Sensors Journal*, vol. 22, no. 12, pp. 11 928–11 939, 2022.
- [13] S. Rimbart, D. Trocellier, and F. Lotte, "Impact of the baseline temporal selection on the ERD/ERS analysis for Motor Imagery-based BCI," in *EMBC 2023 - 45th Annual International Conference of the IEEE Engineering in Medicine and Biology Society*, Sydney, Australia, Jul. 2023.
- [14] S. Mohdiwale, M. Sahu, G. R. Sinha, and V. Bhateja, "Statistical wavelets with harmony search- based optimal feature selection of eeg signals for motor imagery classification," *IEEE Sensors Journal*, vol. 21, no. 13, pp. 14 263–14 271, 2021.
- [15] C. F. Blanco-Diaz, J. M. Antelis, and A. F. Ruiz-Olaya, "Comparative analysis of spectral and temporal combinations in csp-based methods for decoding hand motor imagery tasks," *Journal of Neuroscience Methods*, vol. 371, p. 109495, 2022.
- [16] T. Shi, L. Ren, and W. Cui, "Feature extraction of brain–computer interface electroencephalogram based on motor imagery," *IEEE Sensors Journal*, vol. 20, no. 20, pp. 11 787–11 794, 2020.
- [17] S.-H. Park and S.-G. Lee, "Small sample setting and frequency band selection problem solving using subband regularized common spatial pattern," *IEEE Sensors Journal*, vol. 17, no. 10, pp. 2977–2983, 2017.
- [18] Y. Zhang, G. Zhou, J. Jin, X. Wang, and A. Cichocki, "Optimizing spatial patterns with sparse filter bands for motor-imagery based brain–computer interface," *Journal of Neuroscience Methods*, vol. 255, pp. 85–91, 2015. [Online]. Available: <https://www.sciencedirect.com/science/article/pii/S016502701500285X>
- [19] S. Brandl, K.-R. Müller, and W. Samek, "Alternative csp approaches for multimodal distributed bci data," in *2016 IEEE International Conference on Systems, Man, and Cybernetics (SMC)*, 2016, pp. 003 742–003 747.
- [20] Y. Park and W. Chung, "Selective feature generation method based on time domain parameters and correlation coefficients for filter-bank-csp bci systems," *Sensors*, vol. 19, no. 17, 2019.

- [21] M. Norizadeh Cherloo, H. Kashеfi Amiri, and M. R. Daliri, "Ensemble regularized common spatio-spectral pattern (ensemble rcssp) model for motor imagery-based eeg signal classification," *Computers in Biology and Medicine*, vol. 135, p. 104546, 2021.
- [22] N. Alizadeh, S. Afrakhteh, and M. R. Mosavi, "Multi-task eeg signal classification using correlation-based imf selection and multi-class csp," *IEEE Access*, vol. 11, pp. 52 712–52 725, 2023.
- [23] G. Prasad *et al.*, "Applying a brain-computer interface to support motor imagery practice in people with stroke for upper limb recovery: a feasibility study," *Journal of NeuroEngineering and Rehabilitation*, vol. 7, no. 1, p. 60, 2010.
- [24] A. Chowdhury, Y. K. Meena, H. Raza, B. Bhushan, A. K. Uttam, N. Pandey, A. A. Hashmi, A. Bajpai, A. Dutta, and G. Prasad, "Active physical practice followed by mental practice using bci-driven hand exoskeleton: A pilot trial for clinical effectiveness and usability," *IEEE Journal of Biomedical and Health Informatics*, vol. 22, no. 6, pp. 1786–1795, 2018.
- [25] A. Chowdhury and J. Andreu-Perez, "Clinical brain-computer interface challenge 2020 (cbcic at wcci2020): Overview, methods and results," *IEEE Transactions on Medical Robotics and Bionics*, vol. 3, no. 3, pp. 661–670, 2021.
- [26] P. Welch, "The use of fast fourier transform for the estimation of power spectra: A method based on time averaging over short, modified periodograms," *IEEE Transactions on Audio and Electroacoustics*, vol. 15, no. 2, pp. 70–73, 1967.
- [27] Y. Meirovitch, H. Harris, E. Dayan, A. Arieli, and T. Flash, "Alpha and beta band event-related desynchronization reflects kinematic regularities," *J. Neurosci.*, vol. 35, no. 4, pp. 1627–1637, Jan. 2015.
- [28] A. Chowdhury, A. Dutta, and G. Prasad, "Corticomuscular co-activation based hybrid brain-computer interface for motor recovery monitoring," *IEEE Access*, vol. 8, pp. 174 542–174 557, 2020.
- [29] S. Roy, D. Rathee, A. Chowdhury, K. McCreddie, and G. Prasad, "Assessing impact of channel selection on decoding of motor and cognitive imagery from MEG data," *Journal of Neural Engineering*, vol. 17, no. 5, p. 056037, oct 2020.
- [30] H. Raza, G. Prasad, and Y. Li, "Ewma model based shift-detection methods for detecting covariate shifts in non-stationary environments," *Pattern Recognition*, vol. 48, no. 3, pp. 659–669, 2015.
- [31] H. Raza, H. Cecotti, Y. Li, and G. Prasad, "Adaptive learning with covariate shift-detection for motor imagery-based brain-computer interface," *Soft Computing*, vol. 20, no. 8, pp. 3085–3096, 2016.